nature portfolio

Peer Review File

Nanofibrous Aerogels with Continuous Conductivity Gradient for Ultrabroadband Absorption-Dominant Electromagnetic Interference Shielding

Corresponding Author: Professor Lizhi Xu

This file contains all reviewer reports in order by version, followed by all author rebuttals in order by version.

Version 0:

Reviewer comments:

Reviewer #1

(Remarks to the Author)
This manuscript presents monolithic all-polymer aerogels with a continuous through-thickness conductivity gradient, enabling ultrabroadband EMI shielding (10.2–40 GHz) with low reflection (R < 0.1) and SE > 30 dB. The experimental work is systematic and supported by modeling. However, the conceptual advance relative to existing gradient-based EMI systems, the practical significance of the relatively large thickness, and the distinctiveness and generality of the fabrication strategy are not yet sufficiently clarified. Substantial strengthening is required before the work can be considered for publication in Nature Communications. I therefore recommend major revision. My detailed comments are as follows:

1. Conductivity or impedance gradients for reflection suppression are already well established in EMI shielding literature, including graded MXene aerogels, CNT-based foams, asymmetric laminates, and multilayer absorbers. The manuscript should more clearly define what constitutes a conceptual advance beyond these prior works.

2. The reported ultrabroadband performance is achieved in samples with thicknesses of several millimeters. For many practical EMI applications, thickness is a key constraint. The authors should clarify how performance scales with reduced thickness, identify the minimum thickness required to maintain R < 0.1 and SE > 30 dB, and discuss whether the observed behavior arises fundamentally from the gradient concept or from sufficient absorption length enabled by relatively thick structures.

3. The conductivity gradient appears to arise naturally from diffusion-limited polymerization. The authors should clarify what aspects of the process are intentionally engineered rather than passive consequences of diffusion. Can the gradient shape be deliberately tailored beyond the intrinsic exponential profile? What distinguishes this strategy from conventional diffusion-induced concentration gradients in porous systems?

4. The manuscript presents this as a general gradient-engineering platform, yet experimental validation is limited to PPy within ANF scaffolds. The authors should clarify the boundary conditions of generality, including compatibility with other conductive polymers, scaffold chemistries, and thickness scales, as well as any scalability limitations.

5. Although A > 0.9 is reported, absorption is inferred from conventional power balance, such as A = 1 − R − T. The manuscript should more clearly distinguish between intrinsic material loss capability and reflection suppression effects. A deeper discussion of dielectric loss, attenuation constants, or comparison with established absorptive materials would strengthen the mechanistic interpretation.

6. All shielding measurements are conducted under normal incidence using waveguide configurations. For broadband EMI applications, angular robustness and polarization independence are critical. The authors should discuss or evaluate performance under oblique incidence and different polarizations to support claims of practical ultrabroadband applicability.

7. The gradient-stratified model is a strong component of the manuscript; however, its predictive value would be enhanced by clearly articulating quantitative design guidelines. Explicit relationships of design parameters such as σ_0, λ, thickness, and target reflection levels would improve the impact and generality of the modeling framework.

8. While mechanical robustness is demonstrated, the manuscript does not fully explore trade-offs between mechanical tuning (e.g., porosity reduction) and electromagnetic performance. The authors should clarify how structural densification influences gradient smoothness, impedance matching, and broadband absorption.

9. Table S2 compares shielding performance with prior reports but does not account for sample thickness, which is a critical parameter for practical EMI applications. Given the millimeter-scale thickness of the present samples, the authors should include thickness-normalized metrics (e.g., SE per unit thickness) to enable a fair and transparent comparison with thinner absorbers and films.

Reviewer #2

(Remarks to the Author)
This manuscript reports nanofibrous aerogels engineered with a continuous through-thickness conductivity gradient to achieve ultrabroadband, absorption-dominant EMI shielding. By controlling diffusion/in situ polymerization of the conductive phase within an ANF-based porous scaffold, the design creates a low-conductivity incident surface for improved impedance matching and a higher-conductivity region deeper in the structure for enhanced ohmic dissipation, aiming to deliver high shielding effectiveness with suppressed reflection across a wide GHz band. The authors further support the concept by using a gradient-stratified model to relate σ(z) to the measured S-parameters and by providing demonstrations relevant to mechanical compliance and thermal/aging stability. That said, several points require clarification and strengthening to improve the rigor, reproducibility, and impact of the work:
1. The Introduction positions continuous gradients as the key advance, but the novelty would be stronger if you explicitly distinguish continuous monolithic gradients from “stacked”/“trilayer” or “discrete gradient” designs using a short comparison paragraph (what failure mode each prior approach suffers: interface mismatch, delamination, frequency-sensitive matching, processing complexity).
2. The abstract claims R < 0.1 over 10.2–40 GHz with SE > 30 dB, which is excellent—but please add the sample thickness, incidence direction (low-σ face), and waveguide/VNA method (even in a brief phrase). That prevents ambiguity about boundary conditions and “real-world” deployment.
3. The authors' fit σ(z) with σ(z)=σ0exp(−z/λ). I suggest you report σ0 and λ for every key specimen in the main text (not only Supplementary), and provide a compact “design table” summarizing (porosity, thickness, σ0, λ, SET, R/A at X and Ka). This will greatly increase reproducibility and design transferability.
4. Performance (SET, R, A) depends strongly on thickness, especially across X→Ka. The manuscript frequently compares samples across processing conditions, but the reader needs a clear statement: were thicknesses identical across MCA-1/2/4/6, MCA-94/88/75, and MCA-4*? If not, normalize or discuss thickness sensitivity (even briefly, with a reference to your GSM model).
5. Waveguide measurements are standard, but low-reflection claims can be sensitive to fixture, edge leakage, or sample mounting (PC plates). Please add a short validation note: (i) calibration method, (ii) repeatability across multiple cuts, and (iii) how you ensured the PC plates do not alter S11/S21 beyond “negligible intrinsic shielding.”
6. The authors' mechanistic narrative mixes (a) progressive impedance transition and (b) internal field redistribution leading to ohmic loss. I recommend adding a short “mechanism schematic” or a bullet list of causal steps tied to your Fig. 4h–k outputs, explicitly distinguishing: entry matching → deeper penetration → spatial shift of |E| and σ(z) overlap → peak in σ|E|2 → absorption dominance.
7. The gradient-stratified model discretizes σ(z). But at GHz frequencies in porous composites, the effective response can also depend on ε*(z), porosity, and connectivity. Please state the modeling assumptions clearly: are μ≈μ0 and ε treated as constant? Is σ frequency-independent? If so, provide a short justification and discuss when this approximation might break (e.g., higher loss dispersion at Ka).
8. The authors correctly discuss porosity controlling PPy infiltration and gradient steepness. But later, porosity is also linked to mechanical performance and to the balance between reflection and absorption. Consider adding one paragraph that explicitly separates:
o (i) porosity → diffusion/tortuosity → λ, penetration depth
o (ii) porosity → effective impedance & scattering
o (iii) porosity → mechanical robustness
This will make the design rules less conflated.
9. The manuscript shows strong orientation dependence (high-σ incidence gives high reflection). Add a short “use-case” statement: when do we want reflection-dominant vs absorption-dominant? Also discuss practical assembly: how will users ensure devices are correctly oriented?
10. The authors mention SE decreases modestly after four months and thermal stability beyond 200 °C. Consider adding humidity aging or cyclic thermal/humidity conditioning (or at least acknowledge it as a limitation), because PPy conductivity and interfacial chemistry can drift in humid environments.
11. The kirigami rule “Lc < λ/4” is good, but it would help to show either a quick derivation/intuition or cite a key reference for aperture/cut scattering criteria. Also specify which wavelength you used (free space at mid-band or waveguide?).
12. There are several spots where phrasing/notation could be tightened for precision:
o Use consistent band naming (X/Ku/K/Ka) and frequency ranges everywhere.
o Define “low-σ face”/“high-σ face” once, early, and keep consistent.
o Consider changing “low first derivate” → “low first derivative” (typo) and check derivative discussion wording for clarity.

Reviewer #3

(Remarks to the Author)

This manuscript presents a highly innovative and well-executed study on monolithic all-polymer aerogels with continuous through-thickness conductivity gradients for ultrabroadband, absorption-dominant electromagnetic interference (EMI) shielding. The work combines elegant materials design, meticulous experimental characterization, and robust theoretical modeling. The demonstrated performance, reflection coefficient (R < 0.1) and shielding effectiveness (SE > 30) dB across 10.2–40 GHz, is exceptional and represents a significant advance over state-of-the-art materials. The inclusion of mechanical robustness and processability further enhances its practical relevance. The manuscript is well-written, logically structured, and the conclusions are supported by the data. A few minor issues remain that should be addressed to improve clarity and completeness.

1. Clarify and quantify the gradient-profile fitting (σ(z)=σ0•exp(−z/λ)). In Fig. 2h,i and Supplementary Fig. 10, the exponential fits appear reasonable, but the manuscript does not report the fitted parameters and uncertainty. Please add text or table in SI listing σ0 and λ for the key samples (e.g., MCA-1, -2, -4, -4*, -88, -75), together with fit quality (R2 and/or RMSE).
2. The derivative analysis is conceptually helpful for linking diffusion–reaction to gradient formation, but it reads overly technical for the main narrative. Consider moving the detailed derivative curves and extended mathematical discussion to the SI, while keeping a short, intuitive explanation in the main text emphasizing penetration depth, σ0, and λ.
3. The notation MCA-4* is introduced in Fig. 3 and used before its meaning becomes clear in the later section. Please define MCA-4* in the figure caption or the first in-text mention, including what the asterisk denotes and why it is introduced.
4. Supplementary Table S2 is useful, but comparisons are difficult without thickness and density. Please add: (i) thickness for each benchmark entry (if available) in the references, (ii) density or areal density when reported, and (iii) the frequency band definition used for each metric. Also, please correct the reported bandwidth of this work: the bandwidth corresponding to A > 0.9 should be 29.8 GHz (10.2–40.0 GHz) rather than 3.3 GHz.
5. The phrases “continuous conductivity gradient” and “monolithic gradient” are central but not explicitly defined early. Please add a brief definition in the Introduction, clearly distinguishing them from discrete multilayer/stepwise-gradient designs.
6. The GSM results convincingly show that increasing N in stepwise approximations improves performance. To make the “continuous gradient” advantage more practically irreplaceable, I would suggest to consider adding one layered control sample (e.g., a 3-layer stepwise conductivity-gradient control using the same material system). This can be achieved by stacking thin layers with controlled PPy contents or by stepwise infiltration/polymerization to create discrete interfaces.
7. Unify the naming and definition of λ. The manuscript refers to λ as “decay coefficient/decay character/decay coefficient.” Please standardize to same term (e.g., decay length) and specify units (μm or mm), and the z-axis direction at first use (define z=0 at which surface, and which side is the incident face).
8. Fix symbol formatting consistency and ensure consistent italicization and symbol style throughout, including main texts, methods and supplementary table. Keep the font size and alignment consistent in Supplementary Table 2.
9. In addition to the quantitative parameters (σ0, λ), add a short engineering-style statement summarizing the design rule to improve readability, e.g., lower σ0 improves impedance matching at the incident surface; moderate λ enables gradual transition; excessively small/large λ degrades matching or absorption distribution.

Version 1:

Reviewer comments:

Reviewer #1

(Remarks to the Author)
The paper entitled “Nanofibrous Aerogels with Continuous Conductivity Gradient for Ultrabroadband Absorption-Dominant Electromagnetic Interference Shielding” has been revised. The authors resolved the raised issues in the review process, by clarifying their original contribution, adding the objective comparison with thickness-based metrics, and adding relevant mechanistic validation. The revised manuscript appeals to the broad readers of Nature Communications. Thus, this paper is acceptable at this stage.

Reviewer #3

(Remarks to the Author)
The author has answered my questions point by point and revised the manuscript according to the suggestions. I recommend publishing this manuscript.

REVIEWER COMMENTS

Reviewer #1

Summary: This manuscript presents monolithic all-polymer aerogels with a continuous through-thickness conductivity gradient, enabling ultrabroadband EMI shielding (10.2–40 GHz) with low reflection (R < 0.1) and SE > 30 dB. The experimental work is systematic and supported by modeling. However, the conceptual advance relative to existing gradient-based EMI systems, the practical significance of the relatively large thickness, and the distinctiveness and generality of the fabrication strategy are not yet sufficiently clarified. Substantial strengthening is required before the work can be considered for publication in Nature Communications. I therefore recommend major revision.

Our response: We greatly appreciate your positive comments and suggestions. According to your suggestions, we have made a major revision of the manuscript to further clarify the conceptual advance, the practical significance, and the distinctiveness and generality of the fabrication strategy. The detailed point-by-point replies are shown as follows. We thank you again for helping us improve the manuscript and bring it closer to the standards of *Nature Communications*.

Comments 1-1#:

Conductivity or impedance gradients for reflection suppression are already well established in EMI shielding literature, including graded MXene aerogels, CNT-based foams, asymmetric laminates, and multilayer absorbers. The manuscript should more clearly define what constitutes a conceptual advance beyond these prior works.

Our response: We sincerely thank you for this important comment. The conceptual advance of our work lies in realizing a monolithic all-polymer aerogel with a continuous through-thickness conductivity gradient, rather than the stacked, laminated, or stepwise-gradient architectures used in prior studies. This continuous gradient is generated by diffusion-controlled oxidative polymerization of polypyrrole within an aramid nanofiber scaffold, instead of by layer-by-layer assembly or sequential deposition. As a result, our MCAs contain no discrete interlayer boundaries, which helps reduce abrupt internal impedance discontinuities and interlayer delamination risk while providing a smoother impedance transition and distributed attenuation pathway. This architecture enables ultrabroadband absorption-dominated EMI shielding with $R < 0.1$ over 10.2–40 GHz while maintaining $SE > 30$ dB, outperforming previously reported EMI shielding materials. According to your comment, we have added and revised some sentences in the revised manuscript (as follows) to further emphasize the conceptual distinction and advance beyond existing works.

Our revisions to the manuscript: On Page 2, Line 75-82, we modified:

"*Despite these advances, the existing gradient shields are mainly constructed by stacking, asymmetric lamination, sequential deposition, or other discrete-gradient routes*[14,16,19]. *As a result, their conductivity profiles are often stepwise rather than truly continuous, and the* *retained interlayer boundaries may introduce local impedance discontinuities, imperfect interfacial contact, and delamination risk. Moreover, their low-reflection response can be sensitive to layer thickness and stacking sequence, potentially limiting the effective matching bandwidth, while multistep assembly adds processing complexity*."

On page 12, Line 471-475, we modified:

"*We have established a monolithic conductivity-gradient engineering strategy through diffusion-reaction coupled in situ polymerization to achieve ultrabroadband, absorption-dominated EMI shielding in lightweight all-polymer aerogels. Compared with stacked or stepwise-gradient architectures, the interface-free continuous gradient mitigates abrupt impedance discontinuities and eliminates interlayer delamination.*"

Comments 1-2#:

The reported ultrabroadband performance is achieved in samples with thicknesses of several millimeters. For many practical EMI applications, thickness is a key constraint. The authors should clarify how performance scales with reduced thickness, identify the minimum thickness required to maintain R < 0.1 and SE > 30 dB, and discuss whether the observed behavior arises fundamentally from the gradient concept or from sufficient absorption length enabled by relatively thick structures.

Our response: Thank you for the comment. We have clarified the distinction between the sample thickness and the effective gradient length defined as the PPy-containing gradient region. In our current sample library, the bulk MCAs used for broadband low-reflection shielding have a thickness of ~5 mm. The optimized MCA-4* is the experimentally validated configuration that simultaneously maintains $R < 0.1$ and $SE > 30$ dB over 10.2–40 GHz. Therefore, in the present design, ~5 mm is the minimum validated thickness for meeting both criteria, but it is not a universal lower limit.

Within the experimental ranges, reducing the effective gradient length increases reflection. For example, shortening the diffusion/reaction time reduces PPy penetration from ~4.0 to ~2.5 mm, and the absorption coefficient decreases from 0.84 to 0.76. Lowering the scaffold porosity further confines the gradient thickness to ~2.0 mm and reduces A to 0.67, although SE remains above 30 dB.

Stepwise thinning experiments of a representative gradient sample also show that removing the low-σ entrance region greatly increases R, whereas SE_T changes only modestly (Supplementary Fig. 12). These results indicate that the low-σ gradient region primarily governs impedance matching and absorption–reflection partitioning. In other words, the gradient concept efficiently controls the observed absorption-dominant EMI shielding behavior. Furthermore, to distinguish the gradient effect from thickness alone, we compared MCA-4* with a similarly thick non-gradient control made from stacked uniform aerogel slabs. The non-gradient control achieves high SE (>50 dB) but remains reflection-dominated with $R > 0.8$ (Supplementary Fig. 13), whereas the gradient MCA-4* achieves $R < 0.1$ and $A > 0.9$. Thus, sufficient thickness provides attenuation length that helps maintain high SE, but the continuous conductivity gradient is essential for low-reflection entry and absorption-dominated shielding. We have revised the manuscript to clarify this gradient–thickness synergy.

Our revisions to the manuscript: According to the reviewer's suggestion, we revised the Results section on Page 7, Line 272-283:

"*To explore the effect of the conductivity-gradient region and thickness, we combined stepwise trimming experiments with simulations (Supplementary Fig. 12). In a representative ~5-mm-thick gradient MCA under low-σ-face incidence, R was initially 0.15. Sequential removal from the low-σ face until only the 1 mm-thick high-σ layer remained increased R from 0.15 to 0.8, while the SE changed only slightly. Thus, the gradient region governs the absorption–reflection partition, whereas the high-σ region largely preserves transmission blocking. By contrast, non-gradient controls of comparable thickness achieved* $SE_T > 50dB$ *but retained high reflectivity R > 0.8, showing little tunability in the absorption-reflection-transmission partitioning (Supplementary Fig. 13). These results indicate that the low-reflection response arises primarily from continuous-gradient enabled impedance matching rather than thickness alone*."

In the Supplementary Information, we have added the following statement to the caption for Supplementary Fig. 10 on Page 11:

"*To assess thickness effects, we distinguish the sample thickness from the effective gradient length defined as the PPy-containing gradient region. Unless otherwise noted, the bulk MCAs compared in Fig. 3e–g and Supplementary Table 1 had the same thickness of ~5 mm. Shortening the diffusion/reaction time reduced the gradient length from ~4.0 to ~2.5 mm and decreased A from 0.84 to 0.76, while lowering the scaffold porosity further confined the gradient length to ~2.0 mm and reduced A to 0.67. In both cases,* SE_T *remained above 30 dB, indicating that millimeter-scale conductive thickness can provide low EMW transmission but does not by itself ensure low reflection. In the present experimentally validated design, 5 mm is the minimum nominal thickness confirmed to satisfy both R < 0.1 and* SE_T *> 30 dB over 10.2–40 GHz.*"

Comments 1-3#:

The conductivity gradient appears to arise naturally from diffusion-limited polymerization. The authors should clarify what aspects of the process are intentionally engineered rather than passive consequences of diffusion. Can the gradient shape be deliberately tailored beyond the intrinsic exponential profile? What distinguishes this strategy from conventional diffusion-induced concentration gradients in porous systems?

Our response: We are grateful for your comment. The through-thickness conductivity gradient originates from a diffusion-reaction coupling process: the oxidant diffuses from the top surface into the monomer-infused porous scaffold and triggers oxidative polymerization in a spatially confined manner, leading to a monotonic, smooth PPy distribution that can be parameterized by an exponential form, $\sigma(z)=\sigma_0 \exp(-z/\lambda)$.

Rather than passive consequences of diffusion, we intentionally engineer the gradient characteristics mainly by controlling (i) diffusion/reaction time, (ii) scaffold porosity/tortuosity, and (iii) reaction environment, which jointly tune σ_0, λ, and the effective penetration depth.

More complex non-exponential or non-monotonic gradients would require additional processing degrees of freedom, such as staged multi-step infiltration/polymerization or multi-sided feeding, and therefore lie beyond the scope of the present single-step strategy.

Instead, our one-step, top-fed, diffusion-limited, polymerization yields an exponential-like family of gradients with tunable σ_0 and λ.

Our strategy is fundamentally distinct from conventional diffusion-induced concentration gradients in porous media. Traditional approaches typically create a gradient of mobile solute concentration that may relax toward uniformity unless externally "frozen." In our case, diffusion is coupled to an in-situ chemical reaction that converts monomers into insoluble PPy and immobilizes it as a conformal coating on the nanofibrous scaffold via strong interfacial interactions, thereby "writing" a continuous conductive network gradient (functional conductivity gradient) into a monolithic aerogel rather than merely imposing a transient concentration gradient.

Our revisions to the manuscript: According to your comment, we have modified the following sentences.

On Page 5, Line 188-189, we added:

"*The through-thickness concentration gradient is established by diffusion-reaction coupling*."

On Page 6, Line 200-203, we added:

"*Unlike conventional diffusion-induced concentration gradients, our gradient is encoded by diffusion-coupled in situ polymerization, which immobilizes insoluble PPy on the nanofibrous scaffold to form a continuous conductive network within a monolithic scaffold*."

On Page 6, Line 235-239, we modified:

"*The gradient arises from diffusion-reaction coupling. Rather than passive consequences of coupled diffusion and reaction, we intentionally engineer the conductivity gradient characteristics mainly by controlling (i) diffusion/reaction time, and (ii) scaffold porosity/tortuosity and (iii) reaction environment*."

Comments 1-4#:

The manuscript presents this as a general gradient-engineering platform, yet experimental validation is limited to PPy within ANF scaffolds. The authors should clarify the boundary conditions of generality, including compatibility with other conductive polymers, scaffold chemistries, and thickness scales, as well as any scalability limitations.

Our response: We thank you for this important comment. We have revised the manuscript to clarify the boundary conditions of generality, including the employment of PPy, compatibility with other scaffold chemistries, and thickness scales, as well as any scalability limitations.

To evaluate scaffold compatibility, we added Supplementary Fig. 16, showing that one-sided oxidative polymerization of pyrrole forms visible PPy gradients in silk fibroin, ANF, PVA, and bacterial-cellulose hydrogel scaffolds. As a representative non-ANF example, silk fibroin–PPy gradient aerogels show direction-dependent X-band EMI shielding, with lower reflection and higher absorption under low-conductivity-face incidence, consistent with the ANF-PVA/PPy MCAs. These results support scaffold-level compatibility of the PPy diffusion–reaction route. Extension to other conductive polymers remains to be validated and would require compatible polymerization chemistry, diffusion kinetics, and polymer retention within the scaffold, which will be investigated in future work.

We also clarify thickness and scale-up limits. In the ANF-PVA/PPy system studied here, the PPy penetration depth was tuned from ~2.0 to ~4.0 mm by diffusion time and scaffold porosity within 5 mm monoliths. Theoretically, thinner gradients can be targeted by shorter diffusion/reaction times and more tortuous scaffolds, and larger gradient depths require more open scaffolds and/or longer diffusion. For scale-up, larger-area samples should be feasible by scaling the one-sided precursor-delivery and drying setup, with the practical size currently limited by mold design and supercritical-drying capacity.

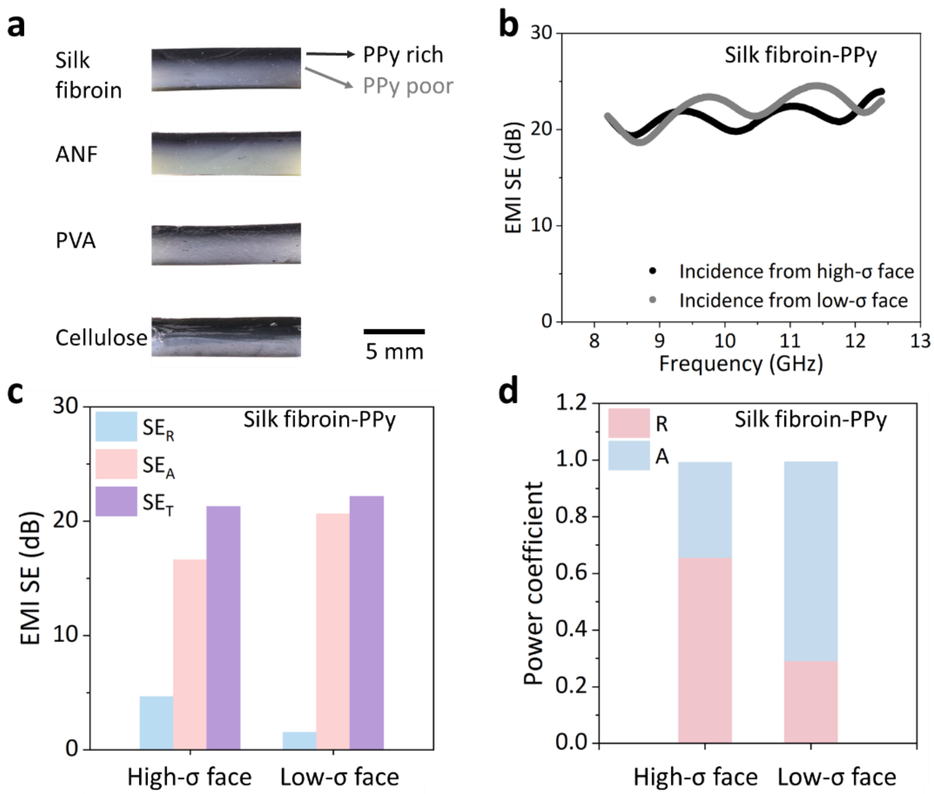

Supplementary Fig. 16 Scaffold-level compatibility of PPy gradient formation. a. In situ growth of PPy in different porous scaffolds, including silk fibroin, ANF, PVA, and bacterial-cellulose hydrogel, forming visible PPy gradients. b-d, EMI shielding properties of a representative silk fibroin–PPy gradient aerogel: (b) EMI *SE* across the X band; (c) SE_A, SE_R, and SE_T; and (d) power coefficients for incidence from the low-conductivity and high-conductivity faces.

Our revisions to the manuscript:

On Page 9, Line 338-341, we modified:

"*The PPy route also produced visible gradients in silk fibroin, ANF, PVA, and bacterial-cellulose scaffolds, indicating scaffold-level compatibility, although extension to other conductive polymers requires validation (Supplementary Fig. 16).*"

In the Supplementary Information, we have added the following statement to the caption for Supplementary Fig. 16 on Page 17-18:

"*To probe scaffold-level compatibility, we applied an analogous one-sided Py/$FeCl_3$ reaction–diffusion process to chemically distinct wettable porous scaffolds, including silk fibroin, ANF, PVA, and bacterial-cellulose hydrogel. All samples developed visible dark-to-light PPy distributions, consistent with gradient deposition. As a representative non-ANF system, the silk fibroin–PPy gradient aerogel was further evaluated for EMI shielding. The silk fibroin–PPy aerogel exhibited comparable X-band total SE_T under opposite incident directions, but showed direction-dependent shielding contributions: low-σ-face incidence resulted in lower reflection and higher absorption than high-σ-face incidence. These results support the scaffold-level compatibility of the PPy reaction–diffusion route and indicate that the asymmetric absorption-dominated shielding behavior can be retained in a non-ANF scaffold.*

For the aqueous PPy system, successful gradient formation requires a wettable, structurally stable porous monolith that allows through-thickness monomer/oxidant transport and retains nascent PPy before complete precursor homogenization. The effective gradient depth can be tuned by diffusion–reaction conditions and scaffold tortuosity, while the monolithic thickness should exceed the targeted gradient length. Larger-area samples should be feasible by scaling the one-sided precursor-delivery and drying setup, with the practical size limited by mold design and supercritical-drying capacity."

Comments 1-5#:

Although A > 0.9 is reported, absorption is inferred from conventional power balance, such as A = 1 − R − T. The manuscript should more clearly distinguish between intrinsic material loss capability and reflection suppression effects. A deeper discussion of dielectric loss, attenuation constants, or comparison with established absorptive materials would strengthen the mechanistic interpretation.

Response: We sincerely thank you for this comment. The high absorptance of MCA-4*, characterized by A ~ 0.91, R ~ 0.09, and $SE_T > 30$ dB, arises from both strong internal attenuation and gradient-enabled reflection suppression. Owing to the high conductivity of the MCA aerogel (> 100 S m^{-1}), the apparent complex permittivity is strongly affected by conduction, and accurate measurement of its complex permittivity is highly challenging with the current experimental setup. Therefore, we did not attempt to derive dielectric loss parameters or attenuation constant from complex permittivity in the present revision, as commonly reported for conventional EMW-absorbing materials (reference: doi:10.1038/s41467-022-28906-4, *Nat. Commun*. 2022, **13**, 1227). Instead, to provide a clearer and complementary evaluation of the internal attenuation and reflection contributions, we further analyzed the shielding effectiveness by absorption (SE_A) and reflection (SE_R), which is commonly reported in EMI shielding materials to discuss internal attenuation and front-surface reflection (see references: doi:10.1038/s41586-025-09699-0, *Nature* 2025, **647**, 356-363; doi:10.1126/science.aba7977, *Science* 2020, **369**, 446-450). In conventional EMI-shielding analysis, SE_A reflects attenuation of the wave fraction entering the shield, arising from internal loss processes such as dipolar/interfacial polarization and conductive loss, whereas SE_R is associated with impedance mismatch and mobile-carrier-induced reflection.

As shown in Fig. 4b-d, under low-σ-face incidence, MCA-4* shows a very small SE_R of 0.4 dB and a high SE_A of 31.9 dB in the X band, together with $R{\sim}0.09$, $A{\sim}0.91$, and negligible $T{\sim}6.0 \times 10^{-4}$. The high SE_A indicates that the wave fraction entering the aerogel is strongly attenuated internally, mainly through PPy-network ohmic loss assisted by dielectric/interfacial polarization. Meanwhile, the low SE_R and low R indicate suppressed conductivity-induced front-surface reflection, thus allowing the incident wave to enter the lossy interior.

Our reverse-incidence result further confirms that high internal loss alone does not guarantee high absorptance; reflection suppression by impedance matching is also required. Under high-σ face incidence, MCA-4* still shows strong internal attenuation ($SE_A{\sim}22.9\ dB$) and negligible transmission, but SE_R and R increase to 9.5 dB and 0.89. This behavior is consistent with reported EMI shields, in which high SE_A can coexist with high $R > 0.5$ (or $SE_R > 3$ dB) due to a lack of surface-impedance matching. (see references: DOI: 10.1126/sciadv.abj1663, *Sci. Adv.* 2021, **7**, eabj1663; doi: 10.1002/adma.202311135, *Adv. Mater.* 2024, **36,** 231113; doi: 10.1002/adma.201908496, *Adv. Mater.* 2020*,* **32**, 1908496).

The gradient-stratified model (GSM) based loss profiles further support this mechanism (Fig. 4h-j). For low-σ-face incidence, the low-σ entrance enables field penetration, and the penetrated field then overlaps with progressively higher local conductivity, producing distributed conductive loss inside the aerogel. Therefore, the high absorption arises from the combination of gradient-enabled reflection suppression and internal ohmic attenuation.

Our revisions to the manuscript: To further strengthen the mechanistic interpretation, we have revised the manuscript to distinguish between reflection suppression and internal attenuation.

On Page 9-10, Line 364-373, we revised:

"*For a representative exponential gradient, MCA-4* under low-σ face incidence shows SE_R ~ 0.4 dB and a SE_A ~ 31.9 dB, together with R ~ 0.09, A ~0.91, and negligible T. The high SE_A indicates strong internal attenuation of the coupled waves, mainly through PPy-network ohmic loss assisted by dielectric/interfacial polarization, whereas the low SE_R and R indicate suppressed front-surface reflection through impedance matching. Reversing the incidence to the high-σ face preserves transmission blocking (SE_T ~32.4 dB) but increases SE_R and R to ~ 9.5 dB and 0.89, respectively, while decreasing A to ~ 0.11. Simulated and experimental trends agree in both orientation and magnitude, indicating that absorption-dominated shielding requires both strong internal attenuation and reflection suppression.*"

Comments 1-6#:

All shielding measurements are conducted under normal incidence using waveguide configurations. For broadband EMI applications, angular robustness and polarization independence are critical. The authors should discuss or evaluate performance under oblique incidence and different polarizations to support claims of practical ultrabroadband applicability.

Our response: We sincerely thank you for raising the constructive point. In this work, the EMI shielding performance was characterized using the standard waveguide method (TE_{10} mode), which is widely used in the research of low-reflection EMI shielding materials. It should be noted that this testing method corresponds to normal incidence, and therefore, it does not allow for direct control of the incident angle in the experimental test. To address the point about oblique incidence and polarization dependence, we have added an electromagnetic simulation analysis to the revised manuscript.

We investigated the material's EMI shielding performance at incident angles of 0°, 30°, and 60° under both TE and TM polarization modes, including SE_A, SE_R, SE_T, absorption (A), reflection (R), and transmission (T) (Supplementary Fig. 14). The results show that the transmission remains very low throughout 8.2–12.4 GHz under all tested conditions ($SE_T > 30$ dB), while absorption remains the dominant shielding channel in all cases ($A > R$). Although the relative contributions of absorption and reflection vary with incident angle and polarization, the overall shielding response remains robust under both TE and TM excitations.

Our revisions to the manuscript: We have added supplementary Fig. 14 and the corresponding discussion in the revised manuscript.

On Page 9, Line 330-333, we added:

"*Angle- and polarization-resolved simulations confirmed absorption-dominated shielding ($SE_T > 30$ dB, $A > R$) across 8.2–12.4 GHz for both TE and TM incidence up to 60° (Supplementary Fig. 14).*"

In the Supplementary Information, we have added the following statement to the caption for Supplementary Fig. 14 on Page 15:

"*To evaluate the shielding robustness beyond the waveguide configuration, we performed full-wave simulations under oblique incidence at 0°, 30°, and 60° for both TE and TM polarizations. The frequency-dependent A, R, and T responses remain stable over 8.2–12.4 GHz. In all cases, T is strongly suppressed and remains negligible ($T < 0.08\%$), indicating that the incident electromagnetic waves are effectively attenuated within the gradient shielding material. Although the relative proportions of absorption and reflection vary with incident angle and polarization, absorption consistently dominates over reflection ($A > R$), confirming the absorption-dominated shielding mechanism. This trend is further supported by the corresponding shielding-effectiveness analysis, where the total shielding effectiveness (SE_T) is mainly contributed by absorption shielding effectiveness (SE_A), while reflection shielding effectiveness (SE_R) remains comparatively small. These results demonstrate that the gradient architecture maintains robust EMI shielding under oblique incidence and different polarization states, highlighting its effectiveness in practical electromagnetic environments beyond the ideal waveguide configuration*."

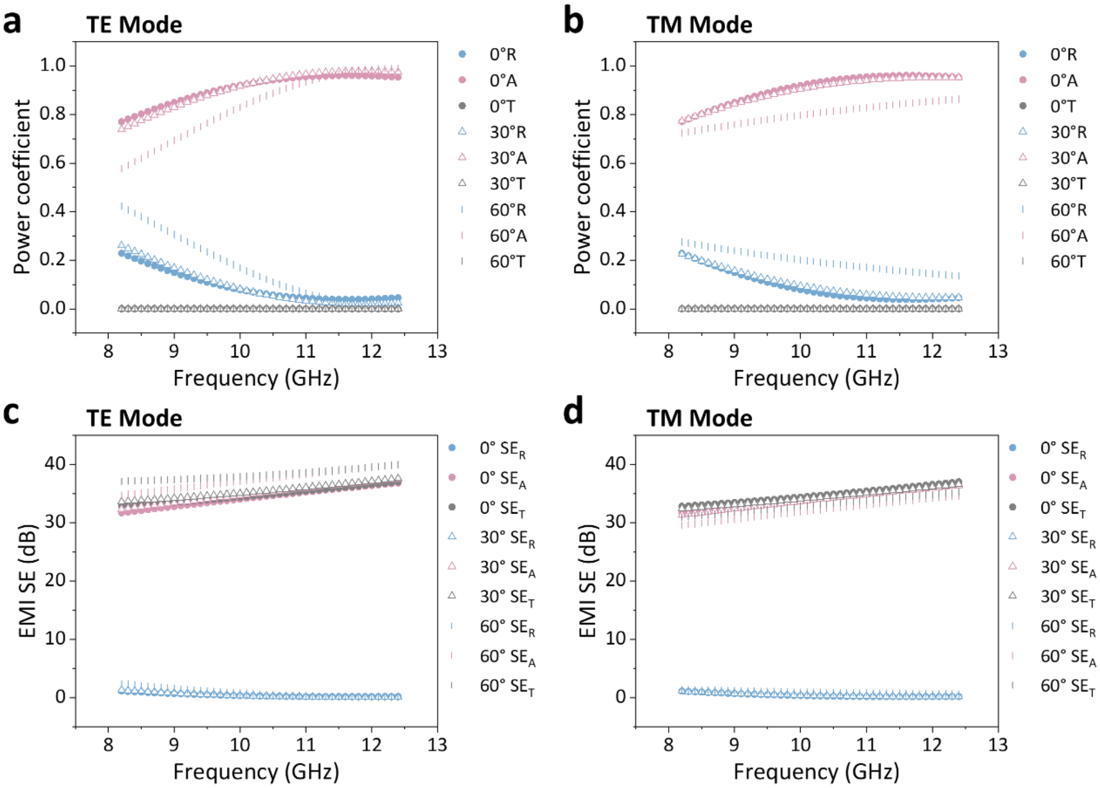

Supplementary Fig. 14 Simulated oblique-incidence EMI shielding response under TE and TM polarizations. Frequency-dependent absorption (*A*), reflection (*R*), and transmission (*T*) of the gradient shielding material under (a) TE and (b) TM polarizations, together with the corresponding shielding-effectiveness components, including reflection shielding effectiveness (SE_R), absorption shielding effectiveness (SE_A), and total shielding effectiveness (SE_T), under (c) TE and (d) TM polarizations. The data are shown at incident angles of 0°, 30°, and 60° over 8.2–12.4 GHz.

Comments 1-7#:

The gradient-stratified model is a strong component of the manuscript; however, its predictive value would be enhanced by clearly articulating quantitative design guidelines. Explicit relationships of design parameters such as σ_0, λ, thickness, and target reflection levels would improve the impact and generality of the modeling framework.

Our response: We sincerely thank you for this comment. We agree that the predictive value of the GSM can be stated more explicitly in terms of quantitative design rules.

In the revised manuscript, we expanded Supplementary Fig. 20 to include simulated 3D maps of SE_T and *A*, as well as *T* and *R*, as functions of σ_0 and λ at thickness (d) of 5 mm and 10 GHz under low-σ-face incidence. We also revised the text to make the target-level design criteria explicit. For the exponential profile $\sigma(z) = \sigma_0 \exp(-z/\lambda)$, where $z = 0$ is defined at the high-σ surface, the conductivity at the low-σ incident face is $\sigma_{inc} = \sigma_0 \exp(-d/\lambda)$. Thus, thickness enters the design relation through *d*, while the present maps are design maps with *d* fixed at 5 mm.

In Fig. 4e-g and Supplementary Fig. 20, the maps reveal three design regimes. First, low σ_0 and/or overly small λ gives insufficient distributed loss, resulting in high T and inadequate SE_T. Second, excessive σ_0 or overly large λ suppresses T but reintroduces entrance-side impedance mismatch, leading to higher R. Third, an intermediate σ_0–λ window simultaneously suppresses both T and R, producing high absorption. Because $A = 1 - R - T$, a SE_T target ≥ 30 dB corresponds to $T \leq 10^{-3}$; therefore, within the low-T regime, the target $R \leq 0.1$ is essentially equivalent to $A \geq 0.899$, i.e., $A > 0.9$. This explains why the high-A window overlaps with the low-R design window on maps in low-T regimes.

Experimentally, MCA-4* lies within this intermediate design σ_0–λ window, with σ_0 ~ 350 S m^{-1} and λ ~ 450 μm at d ~ 5 mm, giving a simulated X-band SE_T of 32.3 dB, R of 0.09, and A of 0.91. We further evaluated the effects of gradient region and thickness by thinning experiments in Supplementary Fig. 12, which shows that reducing thickness from the low-σ face mainly increases R and decreases A, while SE_T changes more modestly in the X band. In contrast, non-gradient controls of comparable thickness (~5 mm) achieved $SE_T > 50$dB but retained high reflectivity R > 0.8. We have revised the manuscript to state these design relationships more directly.

Our revisions to the manuscript:

To better explicit relationships of design parameters such as σ_0, λ, thickness, and target reflection levels, we expanded Supplementary Fig. 20 to include simulated 3D maps of not only SE_T and A, but also T and R, as functions of σ_0 and λ at d = 5 mm and 10 GHz under low-σ face incidence. We have also revised sentences to improve clarity of the manuscript.

On Page 10, Line 374-388, we revised:

"*We model the through-thickness conductivity as $\sigma(z) = \sigma_0 \exp(-z/\lambda)$, with z measured from the high-σ surface (Fig. 4e). At fixed thickness d of 5 mm, frequency of 10 GHz, under low-σ-face incidence, the GSM yields a design map in the explored σ_0−λ space for SE_T, A, T, and R (Fig. 4f,g and Supplementary Fig. 20). Within this range, SE_T increases monotonically with σ_0 or λ (Fig. 4f, Supplementary Fig. 20a), as higher conductivity loading and longer conductive penetration suppress transmission[48]. However, the A and R responses are non-monotonic. R and A maps show that high-A/low-R window (A>0.9 or R<0.1) emerges only at intermediate values of σ_0 and λ (Fig. 4g, Supplementary Fig. 20b,d). Too low σ_0 or too small λ weakens the distributed in-depth loss and leaves transmission insufficiently suppressed, whereas too high σ_0 or too large λ may reintroduce the entrance mismatch and reflection. Thus, the optimal design requires simultaneous entrance matching and internal dissipation. The experimentally optimized MCA-4* falls within this window, consistent with its low R and high SE_T. The GSM thus provides a quantitative basis for optimizing experimentally accessible σ_0–λ combinations, in qualitative agreement with the experimental MCA library.*"

In the Supplementary Information, we have added the following statement to the caption for Supplementary Fig. 20 on Page 21:

"*The maps reveal three design regimes. First, low σ_0 and/or overly small λ gives insufficient distributed loss, resulting in high T and inadequate SE_T. Second, excessive σ_0 or overly large λ suppresses T but increases incident-side σ, reintroducing entrance-side impedance mismatch thereby increasing R. Third, an intermediate σ_0–λ window simultaneously* *suppresses T and R, producing high absorption. Because $A = 1 - R - T$, a SE_T target > 30 dB corresponds to $T \leq 10^{-3}$; therefore, within the low-T regime, the target $R \leq 0.1$ is essentially equivalent to $A \geq 0.899$, i.e., $A > 0.9$. In summary, the maps indicate that the optimal region of high SE_T (≥ 30 dB) with low-R (≤ 0.1)/high-A (> 0.9) occurs only at intermediate σ_0 and λ, where entrance-impedance matching and internal dissipation are simultaneously satisfied.*"

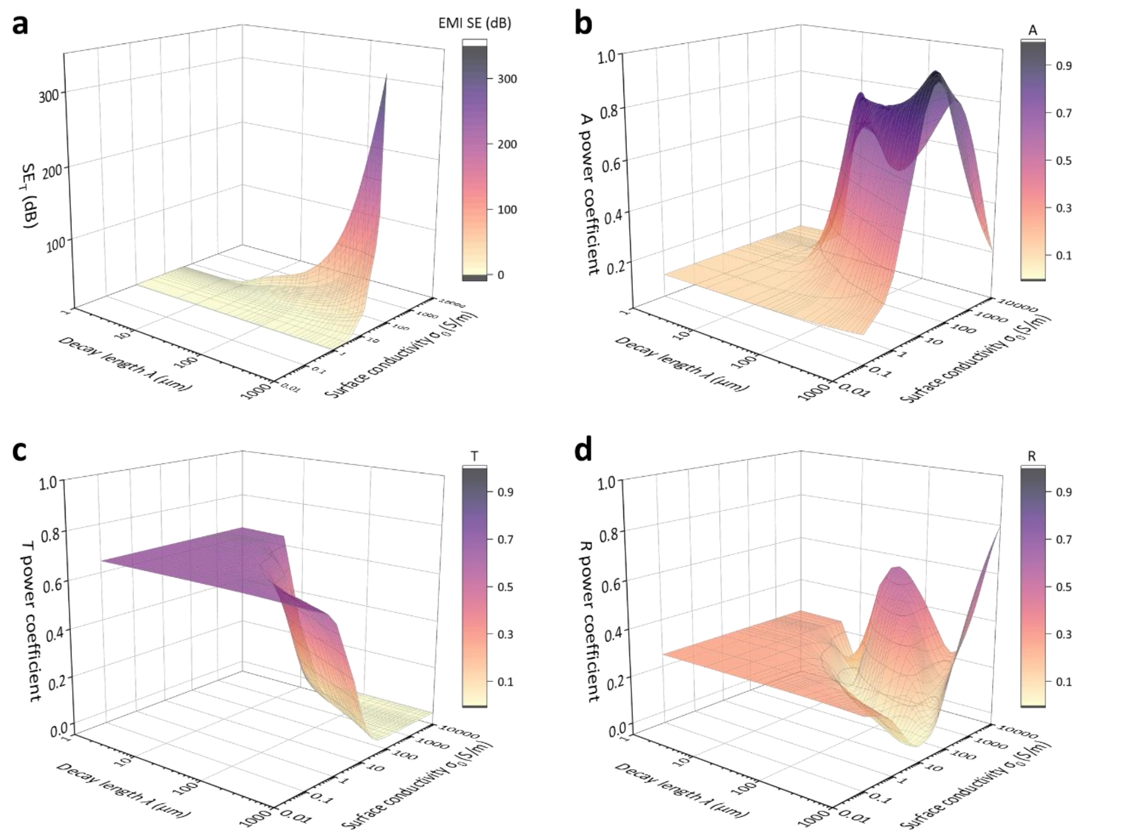

Supplementary Fig. 20 Simulation-derived design maps for conductivity-gradient shields. 3D surface plots showing the dependence of (a) total shielding effectiveness SE_T, (b) absorption power coefficient A, (c) transmission power coefficient T, and (d) reflection power coefficient R on surface conductivity σ_0 and gradient decay length λ for an exponential conductivity profile $\sigma(z) = \sigma_0 \exp(-z/\lambda)$. Simulations were conducted at d = 5 mm and an incident EMW frequency of 10 GHz under low-σ-face incidence.

Comments 1-8#:

While mechanical robustness is demonstrated, the manuscript does not fully explore trade-offs between mechanical tuning (e.g., porosity reduction) and electromagnetic performance. The authors should clarify how structural densification influences gradient smoothness, impedance matching, and broadband absorption.

Our response: Thank you for this important comment. We clarify that lower porosity improves the load-bearing stiffness, strength, toughness, and film integrity of MCAs, but in the present processing window, it also increases transport tortuosity, restricts PPy penetration, reduces λ, and steepens $\sigma(z)$. This makes the impedance transition less gradual and shifts the shielding balance from absorption toward reflection. We further clarify that this is not a universal consequence of densification itself, but a result of the σ_0–λ pair moving away from the GSM-defined high-absorption/low-reflection window. Accordingly, MCA-4* represents the broadband low-reflection/high-absorption design, whereas MCA-75 represents a mechanically robust/high-SE_T design.

We have thus added a concise statement in Section 5 identifying porosity as a coupled electromechanical design parameter, and we provided the detailed quantitative analysis in the caption/discussion of Supplementary Fig. 22 together with Supplementary Tables 1 for discussing about how structural densification influences gradient smoothness, impedance matching, and broadband absorption in the revised manuscript

Our revisions to the manuscript:

On Page 11, Line 419-427, we revised:

"*While EMI performance is often emphasized, practical deployment also requires mechanical robustness, which remains challenging for porous shielding architectures. In the present MCA series, porosity serves as a common control parameter linking gradient formation, the reflection–absorption balance, and mechanical performance. Lower porosity increases tortuosity during in situ polymerization, shortens PPy penetration, and yields a steeper conductivity gradient with a smaller λ. In the current sample series, this shifts the σ_0–λ pair of MCAs away from the high-absorption window identified by the GSM, whereas the denser nanofibrillar network simultaneously enhances load-bearing stiffness, strength, toughness, and film integrity.*"

In the Supplementary Information, we have added the following statement to the caption for Supplementary Fig. 22 on Page 23:

"*Porosity-mediated electromechanical trade-off in MCAs. In the 4 h, ~5 mm porosity-tuned MCA series, decreasing porosity increases diffusion tortuosity and restricts PPy penetration, thereby shortening the conductive-gradient transition and reducing λ. The 94% porosity sample prepared for 4 h, MCA-4/MCA-94, has σ_0 of 900 S m^{-1} and λ of 450 μm, giving SE_T of 49.5 dB, R of 0.16, and A of 0.84. By contrast, MCA-75 has σ_0 of 1100 S m^{-1} and λ of 325 μm, giving higher SE_T of 59.5 dB but larger R of 0.33 and lower A of 0.67. Thus, densification enhances transmission blocking but makes the conductivity transition steeper, weakens progressive impedance matching, and shifts the response from absorption toward reflection in the present processing window. Noted that it is not a universal consequence of densification itself, but a result of the σ_0–λ pair moving away from the GSM-defined high-absorption/low-reflection window. Mechanically, however, the denser nanofibrillar network improves load bearing. The Young's modulus and tensile strength increase from 26 MPa and 1.27 MPa for MCA-94 to 205 MPa and 12.12 MPa for MCA-75. Therefore, MCA-4* represents the broadband low-reflection/high-absorption optimum, whereas MCA-75 represents a superior mechanical robustness and SE_T design.*"

Comments 1-9#:

Table S2 compares shielding performance with prior reports but does not account for sample thickness, which is a critical parameter for practical EMI applications. Given the millimeter-scale thickness of the present samples, the authors should include thickness-normalized metrics (e.g., SE per unit thickness) to enable a fair and transparent comparison with thinner absorbers and films.

Our response: Thank you for this important suggestion. We have added this information to Supplementary Table 3 in the revised Supporting Information, including the sample thickness and thickness-normalized shielding metric for the present work and for prior reports where thickness data are available. For entries in which the relevant parameter was not reported in the original paper, we denote it as "—".

Reviewer #2 (Remarks to the Author):

Summary: This manuscript reports nanofibrous aerogels engineered with a continuous through-thickness conductivity gradient to achieve ultrabroadband, absorption-dominant EMI shielding. By controlling diffusion/in situ polymerization of the conductive phase within an ANF-based porous scaffold, the design creates a low-conductivity incident surface for improved impedance matching and a higher-conductivity region deeper in the structure for enhanced ohmic dissipation, aiming to deliver high shielding effectiveness with suppressed reflection across a wide GHz band. The authors further support the concept by using a gradient-stratified model to relate σ(z) to the measured S-parameters and by providing demonstrations relevant to mechanical compliance and thermal/aging stability. That said, **several points require clarification and strengthening to improve the rigor, reproducibility, and impact of the work:**

Our response: We greatly appreciate your positive comments. According to your suggestions, we have made a revision of the revise manuscript to further improve the rigor, reproducibility, and impact of the work. The detailed point-to-point replies are shown as follows. We thank you again for further improving the manuscript to satisfy the publication in Nature Communications.

Comments #2-1:

The Introduction positions continuous gradients as the key advance, but the novelty would be stronger if you explicitly distinguish continuous monolithic gradients from “stacked”/“trilayer” or “discrete gradient” designs using a short comparison paragraph (what failure mode each prior approach suffers: interface mismatch, delamination, frequency-sensitive matching, processing complexity).

Our response: Thank you for this helpful suggestion. We agree that the novelty is better framed by explicitly distinguishing continuous monolithic gradients from stacked/trilayer/discrete-gradient designs. According to your suggestions, we have revised the following sentences on Page 2, Line 75-82:

Our revisions to the manuscript:

“*Despite these advances, existing gradient shields are mainly constructed by stacking, asymmetric lamination, sequential deposition, or other discrete-gradient routes* [14,16,19]*. As a result, their conductivity profiles are often stepwise rather than truly continuous, and the retained interlayer boundaries may introduce local impedance discontinuities, imperfect interfacial contact, and delamination risk. Moreover, their low-reflection response can be sensitive to layer thickness and stacking sequence, potentially limiting the effective matching bandwidth, while multistep assembly adds processing complexity*.”

Comments #2-2:

The abstract claims $R < 0.1$ over 10.2–40 GHz with $SE > 30$ dB, which is excellent—but please add the sample thickness, incidence direction (low-σ face), and waveguide/VNA method (even in a brief phrase). That prevents ambiguity about boundary conditions and “real-world” deployment.

Our response: Thank you for this helpful suggestion. Accordingly, we have revised the abstract to specify the sample thickness (~5 mm), the incidence direction (low-σ face), and the measurement configuration (VNA-based waveguide method). We have also clarified these conditions in the Methods section.

Our modifications to manuscript:

On page 1, Line 35-40, we modified the sentences as follows:

"*An exponentially decaying conductivity profile enables ultrabroadband, low-reflection performance in 5-mm-thick samples, achieving reflection power coefficient R < 0.1 across 10.2-40.0 GHz, while maintaining shielding effectiveness > 30 dB under low-conductivity face incidence, surpassing existing EMI shields. Waveguide measurements and simulations show that...*"

Comments #2-3:

The authors' fit σ(z) with $\sigma(z)=\sigma_0\exp(-z/\lambda)$. I suggest you report σ_0 and λ for every key specimen in the main text (not only Supplementary), and provide a compact "design table" summarizing (porosity, thickness, σ0, λ, SET, R/A at X and Ka). This will greatly increase reproducibility and design transferability.

Our response: Thank you for this helpful suggestion. We have therefore reported σ_0 and λ for every key specimen in the main text, and added a compact design table, including porosity, thickness, σ_0, λ, together with representative EMI shielding metrics (SE_T, R, A at X and Ka band) in the supplementary information (Supplementary Table 1). Because the systematic specimen library in Fig. 3e–g was compared under identical X-band waveguide conditions, the table reports X-band averaged SE_T, R, and A for all key specimens. For specimens for which broadband measurements are available, we report the Ka-band averaged values; in the present work, this applies to the optimized MCA-4*.

Our modifications to the manuscript:

On Page 6-7, Line 239-250, we revised:

"*... Across the MCA-1/-2/-4/-6 series, increasing the diffusion/reaction time (from 0.75 to 6 h) broadens the conductivity gradient, with λ increasing from 225 to 340, 450, and 485 μm, while σ_0 remains nearly constant at ~900 S m^{-1} (Supplementary Fig. 10a). In contrast, decreasing the scaffold porosity from 94% to 88% and 75% slightly increases σ_0 but steepens the conductivity decay with depth. The σ_0/λ change from ~900 S m^{-1}/450 μm for MCA-4, also noted as MCA-94 in the porosity series, to ~950 S m^{-1}/380 μm for MCA-88 and ~1100 S m^{-1}/325 μm for MCA-75, respectively (Fig. 2g,i and Supplementary Fig. 10b). MCA-4* denotes an intentionally surface-conductivity-reduced variant of MCA-4, prepared under an oxygen-containing polymerization atmosphere; σ_0 decreases to ~350 S m^{-1} while λ remains ~450 μm (Supplementary Fig. 10a,c, Table 1)[43].*"

On Page 8, Line 302-303, we added:

"*The fitted σ_0 and λ values, together with porosity, thickness, and representative shielding metrics, are summarized in Supplementary Table 1.*"

In supplementary information, we added Supplementary Table 1:

Supplementary Table 1 Design table of conductivity gradient parameters and EMI shielding performance of key MCA specimens.

Specimen	Porosity (%)	Thickness (mm)	σ_0 (S/m)	λ (μm)	R^2	X band			Ka band		
						SE_T (dB)	R	A	SE_T (dB)	R	A
MCA-1	94	5	900	225	0.84	42.2	0.24	0.76	—	—	—
MCA-2	94	5	900	340	0.78	46.7	0.19	0.82	—	—	—
MCA-4	94	5	900	450	0.98	49.5	0.16	0.84	—	—	—
MCA-6	94	5	900	485	0.91	52.5	0.22	0.78	—	—	—
MCA-88	88	5	950	380	0.92	54.0	0.28	0.72	—	—	—
MCA-75	75	5	1100	325	0.99	59.5	0.33	0.67	—	—	—
MCA-4*	94	5	350	450	0.94	32.3	0.09	0.91	41.9	0.08	0.92

Note: Values are band-averaged under low-σ-face incidence. X-band: 8.2–12.4 GHz; Ka-band: 26.5–40.0 GHz. R^2 denotes the coefficient of determination for the exponential-profile fit. MCA-4/MCA-94 denotes the 94% porosity sample prepared with a 4 h diffusion/reaction time. MCA-4* denotes the intentionally reduced-surface-conductivity sample derived from MCA-4. "—", not determined; Ka-band data were collected only for the optimized MCA-4* sample used for broadband validation; they were not measured for the X-band screening specimens.

Comments #2-4:

Performance (SET, R, A) depends strongly on thickness, especially across X→Ka. The manuscript frequently compares samples across processing conditions, but the reader needs a clear statement: were thicknesses identical across MCA-1/2/4/6, MCA-94/88/75, and MCA-4*? If not, normalize or discuss thickness sensitivity (even briefly, with a reference to your GSM model).

Our response: Thank you for this important comment. In the revised manuscript, we clarify that the cross-sample comparisons in Fig. 3e–g were made on bulk MCA samples of the same thickness (~5 mm), so the observed differences primarily reflect changes in the conductivity-gradient profile rather than thickness. We also clarify that the broadband X–Ka data in Fig. 3h,i are shown only for the representative MCA-4* sample and are not used for cross-sample comparison. Besides, the effect of the conductivity-gradient region and thickness is discussed explicitly with reference to Supplementary Fig. 12 and 13, where stepwise thinning from the low-σ face shows that reducing thickness/gradient region mainly increases R and decreases A, whereas SE_T changes more modestly in X band. This behavior is consistent with the GSM picture that the low-σ entrance region primarily governs matching and the reflection–absorption partition.

Revisions to the manuscript: We revised the manuscript to distinguish more clearly between gradient-profile effects and thickness effects. On page 8, Line 317-321, we added a brief statement in the Results referring to the thinning experiment and corresponding simulation in Supplementary Fig. 12, which explicitly shows the thickness dependence of SE_T, R, and A.

On Page 7, Line 272-283, we modified:

"…*To explore the effect of the conductivity-gradient region and thickness, we combined stepwise trimming experiments with simulations (Supplementary Fig. 12). For ~5-mm-thick MCAs under low-σ-face incidence, R initially reached 0.15. Sequential removal from the low-σ face until only the 1 mm-thick high-σ layer remained increased R from 0.15 to 0.8, while the SE changed only slightly. Thus, the gradient region governs the absorption–reflection partition, whereas the high-σ region largely preserves transmission blocking. By contrast, non-gradient controls of comparable thickness achieved* $SE_T > 50\,dB$ *but retained high reflectivity R > 0.8, showing little tunability in the absorption-reflection-transmission partitioning (Supplementary Fig. 13). These results indicate that the low-reflection response arises primarily from continuous-gradient enabled impedance matching rather than thickness alone*."

On Page 8, Line 284-286, we modified:

"*We next characterized the X-band shielding response across a library of MCAs (thickness ~5 mm) with varied conductivity gradients (MCA-1, -2, -4, -6, -88, -75, and -4*; Fig. 3e-g).*"

On Page 20, Line 700, we added:

"*All MCA samples in this series were ~5 mm thick*."

On Page 25, Line 820-822, we added in the Methods:

"*Unless otherwise noted, the bulk MCA specimens used for cross-sample comparison were prepared at the same thickness (~5 mm)*."

Comments #2-5:

Waveguide measurements are standard, but low-reflection claims can be sensitive to fixture, edge leakage, or sample mounting (PC plates). Please add a short validation note: (i) calibration method, (ii) repeatability across multiple cuts, and (iii) how you ensured the PC plates do not alter S11/S21 beyond "negligible intrinsic shielding."

Our response: We sincerely thank you for this valuable comment. In this work, EMI shielding performance of MCAs was quantitatively evaluated using a vector network analyzer (VNA, Agilent PNA N5244A) in conjunction with standard rectangular waveguides. Aerogel samples with dimensions of 22.86 × 10.16 mm, 15.8 × 7.9 mm, 10.7 × 4.3 mm, and 7.1 × 3.6 mm were used to cover the X (8.2-12.4 GHz), Ku (12.4-18 GHz), K (18-26.5 GHz), and Ka (26.5-40 GHz) bands, respectively.

To ensure the reliability of the low-reflection measurements, we provide the following validation:

(i) Before measurement, a standard waveguide calibration procedure was performed, which accounts for fixture-related losses and systematic errors, ensuring that all S-parameters are referenced to a well-defined baseline. Specifically, the system was calibrated using a full two-port TRL (Thru-Reflect-Line) procedure with the following standards: 1) Reflect: SHORT on port 1 and SHORT on port 2 (separate connections), 2) Thru: direct connection between port 1 and port 2, 3) Line: a 1/4-wavelength line inserted between port 1 and port 2. The reference planes were set at the waveguide flanges.

(ii) We ensure that we did not add additional cuts to the tested samples; all the SE_T, A, R and T, were calculated from the same S-parameter dataset obtained from each tested specimen. 3–5 independently cut MCA specimens were measured under identical waveguide conditions after separate mounting. The results showed good consistency in EMI *SE* and power coefficients, confirming measurement repeatability and robustness.

(iii) We apologize for the unprecise description of employing PC in the Method section. PC plates were applied only with thin films, especially ultrathin films (see our previous work: doi: 10.1002/adma.201908496, *Adv. Mater.*, 2020, **32**, 1908496; doi:10.1016/j.carbon.2015.10.004, *Carbon*. 2015, **96**, 768-777) in the mention of the mechanical fixture and supporting of thin sample while PC keeping electromagnetic wave transparency (R~0.003, A~ 0.064, T~0.933). For the samples with a certain thickness (~5 mm), samples are not necessary to be supported, thus, we actually did not use PC plate for conducting EMI shielding measurement. We thank you for the careful examination, which allowed us to identify and correct this unprecise description. The corresponding description in the Method has been revised accordingly.

Our revisions to the manuscript: These clarifications have been added to the revised manuscript (Page 24, Line 802–820), confirming that fixture effects, edge leakage, and sample mounting do not compromise the validity of the reported low-reflection performance.

"*The electromagnetic interference (EMI) shielding performance of MCAs was quantitatively evaluated using a vector network analyzer (VNA, Agilent PNA N5244A) in conjunction with a waveguide measurement system. Before each measurement, a full two-port waveguide TRL calibration was performed for the corresponding frequency band. The calibration used standard Thru, Reflect, and Line waveguide standards: the Reflect standard was realized using short plates at the two ports, the Thru standard was obtained by directly connecting the two waveguide ports, and the Line standard was an inserted waveguide section with a known electrical length. The calibration reference planes were set at the waveguide flanges. This procedure removed systematic errors from the VNA, waveguide adapters, and fixture, ensuring that the measured S-parameters were referenced to a well-defined baseline. MCA specimens were cut to match the internal cross-sectional dimensions of standard rectangular waveguides corresponding to the X (8.2-12.4 GHz), Ku (12.4-18.0 GHz), K (18.0-26.5 GHz), and Ka (26.5-40.0 GHz) bands. The in-plane dimensions of the samples were 22.9 × 10.2 mm, 15.8 × 7.9 mm, 10.7 × 4.3 mm, and 7.1 × 3.6 mm, respectively, to ensure precise fitting within the corresponding waveguide apertures and minimize possible edge leakage. To evaluate repeatability, 3–5 independent MCA specimens were measured under identical waveguide conditions after separate mounting. Only specimens that fully filled the waveguide cross-section without visible edge gaps were used.*"

Comments #2-6:

The authors' mechanistic narrative mixes (a) progressive impedance transition and (b) internal field redistribution leading to ohmic loss. I recommend adding a short "mechanism schematic" or a bullet list of causal steps tied to your Fig. 4h–k outputs, explicitly distinguishing: entry matching → deeper penetration → spatial shift of $|E|$ and $\sigma(z)$ overlap → peak in $\sigma|E|2$ → absorption dominance.

Our response: Thank you so much for this suggestion. To address this, we revised Fig. 4 by adding a concise mechanism schematic to the main text and moving the corresponding total electromagnetic energy density plots to the Supplementary Information. The revised figure now links the simulated loss-density profiles directly to the causal sequence for low-σ-face incidence: entry matching → deeper penetration → inward shift of the $| E | - \sigma$ overlap → internal peak in $\sigma | E |^2$ → absorption-dominant shielding. The contrasting high-σ-face case is also clarified as entrance mismatch, shallow penetration, and near-surface loss/reflection.

Our revisions to the manuscript:

On Page 21, we revised Fig. 4 to make the mechanistic sequence more explicit. Specifically, the depth-dependent total electromagnetic energy density plots previously shown in the main figure were moved to Supplementary Information Fig.21, while a new mechanism schematic was added to the main text figure.

On page 10, Line 389-408, we also revised the corresponding discussion to explicitly distinguish entrance matching from internal field redistribution and dissipation：

"*To reveal the mechanism of the conductivity-gradient-enabled electromagnetic behavior, we mapped the depth-dependent field, energy-density, and loss profiles under opposite incidence directions (Fig. 4h,i, and Supplementary Fig. 21). For incidence from the low-σ face, the power loss density profiles show distinct regimes (Fig. 4h). Dielectric polarization dominates near the entrance with low-σ, where |E| is largest. Then, conduction loss prevails deeper inside, as the penetrating wave overlaps with increasing σ(z). Notably, the local conductive loss density,* $p_{loss}(z) \propto \sigma(z)|E(z)|^2$*, exhibits an internal maximum, arising from the competition between the exponential growth of σ(z) and the simultaneous decay of |E| (Supplementary Fig.21b). This behaviour indicates that the continuous gradient not only suppresses front-surface reflection, but also drives the field into the conductive interior, thereby enhancing internal attenuation. By contrast, for high-σ face incidence, the field energy is confined to a shallow entrance region and the loss density decays rapidly with depth (Fig. 4i and Supplementary Fig. 21f,g), consistent with strong interfacial mismatch and reflection-dominated shielding. Together, these results support a two-step mechanism for low-σ-face incidence (Fig. 4j). The low-σ entrance region first improves impedance matching and suppresses front-surface reflection, enabling deeper wave penetration. The penetrated field then overlaps with the inwardly increasing conductivity, causing the local power-loss density,* $p_{loss}(z) \propto \sigma |E|^2$*, to reach an internal maximum and dissipate EM energy through enhanced ohmic loss. This process ultimately leads to absorption-dominated shielding.*"

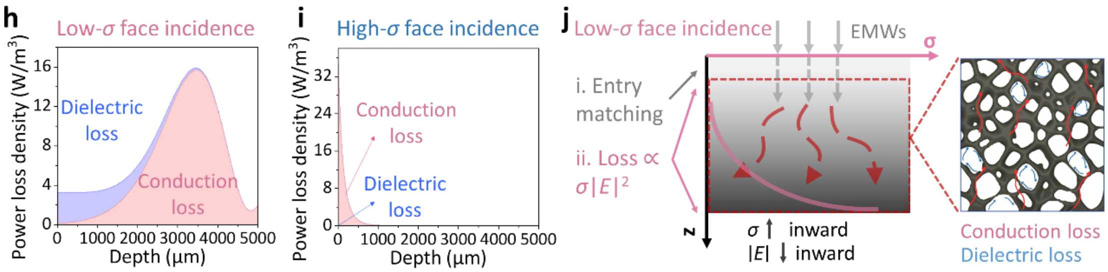

Fig.4 h,i Depth-dependent power-loss density profiles, showing conduction loss and dielectric loss for low- σ -face incidence (**h**) and high- σ -face incidence (**i**). **j** Mechanistic schematic for low-σ-face incidence. Improved entrance matching enables deeper penetration, followed by inward shift of the $|E|-\sigma$ overlap and the formation of an internal peak in $\sigma|E|^2$, which promotes distributed loss and absorption-dominant shielding.

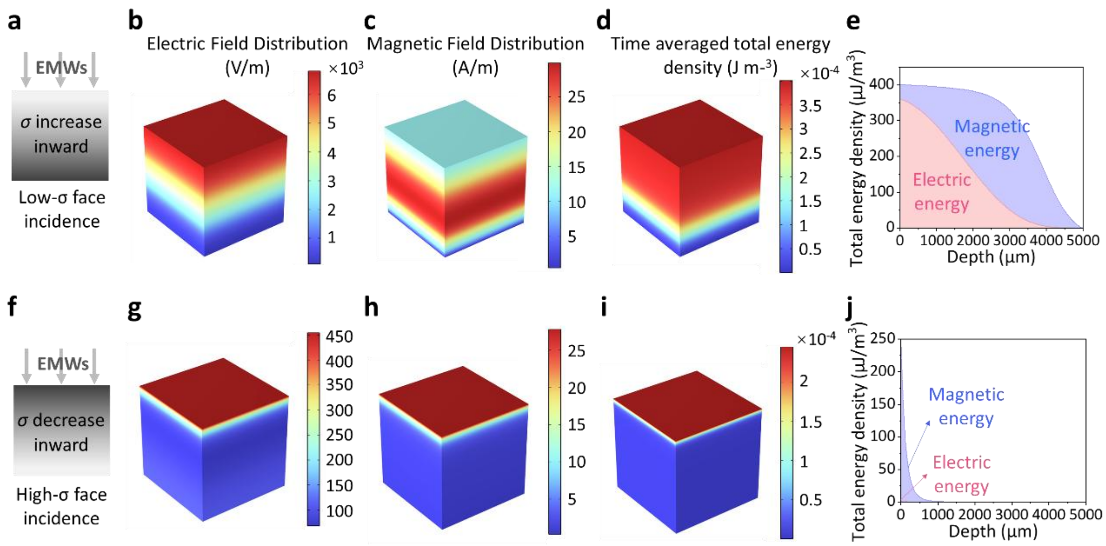

Supplementary Fig. 21 Simulated field, energy-density, and energy-partition distributions for opposite incidence directions in a representative conductivity-gradient MCA at 10 GHz. (a–e) Illustration and simulation results for low-σ-face incidence. a, Schematic showing electromagnetic waves incident from the low-σ surface, where conductivity increases toward the interior. b–d, Three-dimensional distributions of electric-field magnitude $|E|$(b), magnetic-field magnitude $|H|$(c), and time-averaged total electromagnetic energy density (d). e, Corresponding depth-dependent decomposition of total electromagnetic energy into electric and magnetic contributions. (f–j) Illustration and simulation results for high-σ-face incidence. f, Schematic showing incidence from the high-σ surface, where conductivity decreases toward the interior. g–i, Three-dimensional distributions of $|E|$(g), $|H|$(h), and total electromagnetic energy density (i). j, Corresponding depth-dependent decomposition of total electromagnetic energy into electric and magnetic contributions.

In the Supplementary Information, we also added the following statement to the caption for Supplementary Fig. 21 on Page 22:

"*For low-σ face incidence,* $|E|$ *and the total electromagnetic energy density decay gradually through the aerogel, with the energy density decreasing from* 4.01×10^{-4} *to* 1.29×10^{-7} $J\ m^{-3}$ *over 5 mm, corresponding to 34.9 dB attenuation and consistent with the experimentally measured* SE_T*. The attenuation is slow over the first ~3000 μm and then accelerates as the wave reaches more conductive regions and accumulates dielectric and ohmic losses. By contrast, under high-σ face incidence, the field and energy density collapse near the entrance, with the energy density reaching its 1/e value within ~150 μm, consistent with strong entrance-side mismatch and near-surface field confinement. These results support a direction-dependent mechanism in which low-σ face incidence enables progressive impedance matching and absorption-dominated attenuation, whereas high-σ face incidence produces stronger front-surface reflection*."

Comments #2-7:

The gradient-stratified model discretizes σ(z). But at GHz frequencies in porous composites, the effective response can also depend on ε*(z), porosity, and connectivity. Please state the modeling assumptions clearly: are μ≈μ0 and ε treated as constant? Is σ frequency-independent? If so, provide a short justification and discuss when this approximation might break (e.g., higher loss dispersion at Ka).

Response: We sincerely thank you for this suggestion. We agree that, in porous gradient composites at GHz frequencies, the effective electromagnetic response can in principle depend on spatially varying conductivity, complex permittivity, porosity, and network connectivity. We have therefore revised the manuscript to explicitly state the assumptions, justification, and limitations of the gradient-stratified model (GSM).

The GSM is used as a reduced-order effective-medium model to isolate the dominant role of the through-thickness conductivity gradient. Each stratum is treated as a homogeneous and isotropic effective layer, with $\mu_r \approx 1$ for the non-magnetic ANF/PVA/PPy system. For complex permittivity, its imaginary part contains both polarization-related dielectric loss and a conduction contribution. Because the high conductivity of the aerogel strongly affects apparent permittivity and makes it difficult to separate polarization-related dielectric loss from conductive loss, the GSM does not reconstruct a depth-dependent $\varepsilon^*(z,f)$. Instead, $\varepsilon' = 3.5$ and $\tan\delta = 0.07$ are used as a spatially uniform background dielectric response, while conductive loss is introduced separately through the measured $\sigma(z) = \sigma_0 \exp(-z/\lambda)$ profile without explicit frequency dependence. This avoids double counting the conductivity contribution in both ε'' and $\sigma(z)$. Porosity and PPy-network connectivity are treated at the effective-medium level rather than introduced as independent variables. Their contribution is implicitly included in the background dielectric response, while their sample-specific influence is mainly captured by the measured $\sigma(z)$, because porosity and connectivity regulate PPy penetration depth, conductive-network formation, and the resulting σ_0–λ gradient.

We also clarify the limitation of this reduced model. The GSM is primarily used for mechanism analysis and parameter mapping in the X band / at 10 GHz, whereas the ultrabroadband 10.2–40 GHz shielding performance is established experimentally. The constant-ε^*, frequency-independent-σ approximation may become less accurate toward the Ka band or in highly conductive internal regions, where interfacial polarization, hopping/tunneling conduction, and depth-dependent dielectric/conductive dispersion may become important. Thus, at higher frequencies, a full quantitative prediction may require a coupled $\varepsilon^*(z,f)$–$\sigma(z,f)$–porosity/connectivity model.

Our revisions to the manuscript:

We have revised the manuscript accordingly to make these assumptions, justifications, and limitations explicit.

On Page 11, Line 409-415, we added the following paragraph:

"*We note that the present GSM is not intended as a full layer-resolved constitutive model. The constant* ε^**, frequency-independent-*σ *approximation serves as a first-order conductivity-dominant description, which captures the main shielding physics in the X-band/10 GHz mechanism analysis but may become less accurate when stronger loss dispersion is involved, especially toward the Ka band and in the highly conductive deeper region, where interfacial polarization, hopping/tunneling conduction, and* $\varepsilon^*(z,f)$ *variation may become more important*."

On Page 27, Line 908-926, we added the following paragraph:

"*In the GSM, each stratum is treated as a homogeneous and isotropic effective medium. Each layer is* $\mu_r \approx 1$, $\varepsilon_r' = 3.5$, *and* $\tan\delta = 0.07$ *unless otherwise stated. The conductivity is introduced as the only depth-dependent parameter, following the experimentally fitted profile* $\sigma(z) = \sigma_0 \exp(-z/\lambda)$*; no explicit frequency dependence of* σ *is included. This reduced-order treatment absorbs the effects of porosity into the effective constitutive parameters, with the average contribution represented by background dielectric response, whereas sample-specific influence is captured by* $\sigma(z)$*, because porosity and connectivity regulate PPy penetration depth, conductive-network formation, and the resulting* σ_0–λ *gradient. This separation avoids double-counting the conductive contribution in both* ε'' *and* $\sigma(z)$*. The model is intended to isolate the first-order influence of the conductivity gradient on R, A, and T for mechanism analysis and parameter mapping, rather than to reconstruct the full local constitutive response of the graded porous composite*."

In the Supplementary Information, we have added the detailed statement to the caption for Supplementary Fig. 17 on Page 18:

"*Modeling assumptions of the GSM. The present GSM is a reduced-order effective-medium model rather than a full layer-resolved constitutive reconstruction. In the calculations, each stratum is treated as a homogeneous and isotropic effective layer,* μ_r *is taken as ~1,* ε_r^* *is treated as a constant background dielectric response with* $\varepsilon' = 3.5$ *and* $\tan\delta = 0.07$*, and* σ *is described by the experimentally fitted, frequency-independent profile* $\sigma(z) = \sigma_0 \exp(-z/\lambda)$*. Porosity and PPy-network connectivity are not introduced as independent variables, but are implicitly included in the effective parameters, including permittivity and* $\sigma(z)$*. These assumptions isolate the first-order role of the conductivity gradient and capture the main X-band/10 GHz mechanism, including orientation-dependent S-parameters and field/loss redistribution. However, the approximation may become less accurate toward the Ka band or in highly conductive internal regions, where interfacial polarization, hopping/tunneling transport, and depth-dependent* $\varepsilon^*(z,f)$ *and* $\sigma(z,f)$ *dispersion may become important. In such cases, a coupled* $\varepsilon^*(z,f)$–$\sigma(z,f)$*–porosity/connectivity model would be required for quantitative layer-by-layer prediction*."

Comments #2-8:

The authors correctly discuss porosity controlling PPy infiltration and gradient steepness. But later, porosity is also linked to mechanical performance and to the balance between reflection and absorption. Consider adding one paragraph that explicitly separates:

o (i) porosity → diffusion/tortuosity → λ, penetration depth

o (ii) porosity → effective impedance & scattering

o (iii) porosity → mechanical robustness

This will make the design rules less conflated.

Our response: We thank you for this insightful suggestion. In the revised manuscript, we have added a concise clarifying paragraph to separate: (i) porosity-controlled diffusion/tortuosity, which governs PPy penetration depth and the gradient decay length λ; (ii) porosity-related electromagnetic effects, including effective impedance/scattering, while noting that in the present MCAs the dominant experimentally resolved effect is the concomitant change in σ_0 and λ; and (iii) porosity-dependent mechanical robustness arising from densification of the load-bearing nanofibrillar network. We further clarify that the lower absorption of MCA-88 and MCA-75 is not attributed to densification itself, but to the shift of σ_0 and λ away from the high-absorption window predicted by the GSM.

Our revision to the manuscript:

Accordingly, we have added one paragraph on Page 11, Line 419-427.

"*While EMI performance is often emphasized, practical deployment also requires mechanical robustness, which remains challenging for porous shielding architectures. In the present MCA series, porosity serves as a common control parameter linking gradient formation, the reflection–absorption balance, and mechanical performance. Lower porosity increases tortuosity during in situ polymerization, shortens PPy penetration, and yields a steeper conductivity gradient with a smaller λ. In the current sample series, this shifts the σ_0–λ pair of MCAs away from the high-absorption window identified by the GSM, whereas the denser nanofibrillar network simultaneously enhances load-bearing stiffness, strength, toughness, and film integrity*."

In the Supplementary Information, we have added the detailed statement to the caption for Supplementary Fig. 22 on Page 23:

"*Porosity-mediated electromechanical trade-off in MCAs. In the 4 h, ~5 mm porosity-tuned MCA series, decreasing porosity increases diffusion tortuosity and restricts PPy penetration, thereby shortening the conductive-gradient transition and reducing λ. The 94% porosity sample prepared for 4 h, MCA-4/MCA-94, has σ_0 of 900 S m^{-1} and λ of 450 μm, giving SE_T of 49.5 dB, R of 0.16, and A of 0.84. By contrast, MCA-75 has σ_0 of 1100 S m^{-1} and λ of 325 μm, giving higher SE_T of 59.5 dB but larger R of 0.33 and lower A of 0.67. Thus, densification enhances transmission blocking but makes the conductivity transition steeper, weakens progressive impedance matching, and shifts the response from absorption toward reflection in the present processing window. Noted that it is not a universal consequence of densification itself, but a result of the σ_0–λ pair moving away from the GSM-defined high-absorption/low-reflection window. Mechanically, however, the denser* *nanofibrillar network improves load bearing. The Young's modulus and tensile strength increase from 26 MPa and 1.27 MPa for MCA-94 to 205 MPa and 12.12 MPa for MCA-75. Therefore, MCA-4* represents the broadband low-reflection/high-absorption optimum, whereas MCA-75 represents a superior mechanical robustness and SE_T design*."

Comments #2-9:

The manuscript shows strong orientation dependence (high-σ incidence gives high reflection). Add a short "use-case" statement: when do we want reflection-dominant vs absorption-dominant? Also discuss practical assembly: how will users ensure devices are correctly oriented?

Our response: We thank you for this suggestion. As shown in Fig. 3a–d and captured by the GSM in Fig. 4b–d, low-σ-face incidence yields absorption-dominant shielding with suppressed reflection, whereas high-σ-face incidence gives reflection-dominant shielding at nearly unchanged total shielding effectiveness. Therefore, for low-interference shielding where secondary reflection, backscatter, cavity re-radiation, or information leakage must be minimized, the low-σ face should be placed towards the incident-wave or source-facing side. In contrast, when front-surface rejection is preferred and reflected power is acceptable, the high-σ face may be used on the incident side.

We have revised the manuscript to make this use-case distinction explicit. We also clarified practical orientation control: the gradient direction is fixed during one-sided diffusion polymerization and can be identified by intrinsic face-color contrast or rapid surface-conductivity checks.

Our revisions to the manuscript:

Accordingly, we added a short use-case statement on Page 9, Line 326-330.

"*This Janus response enables orientation-specific shielding. Low-σ-face incidence is suited to suppressing secondary reflection, backscatter, and potential information leakage, whereas high-σ-face incidence can be used when front-surface rejection is desired and reflected power is acceptable. The fixed gradient direction can be identified by intrinsic face-color contrast or rapid surface-conductivity checks*."

Comments #2-10:

The authors mention SE decreases modestly after four months and thermal stability beyond 200 °C. Consider adding humidity aging or cyclic thermal/humidity conditioning (or at least acknowledge it as a limitation), because PPy conductivity and interfacial chemistry can drift in humid environments.

Our response: Thank you for this important suggestion. In the revised manuscript, we state that SE decreased from 32 to 28 dB after four months under ambient storage and that no major thermal decomposition was observed below 200 °C, but long-term humid-environment and cyclic hygrothermal stability remain to be established. We also note that moisture-barrier encapsulation and dopant engineering are possible future strategies to improve durability (See references: doi:10.1039/D4MH00494A, *Mater. Horiz*., 2024, **11**, 3792-3804; doi:10.1016/j.corsci.2018.04.021, *Corros. Sci*. 2018, **138**, 252-265).

Our revision to the manuscript:

Accordingly, we have added the discussion on the limitations related to humidity/thermal stability on Page 9, Line 333-338 as follows:

"*Preliminary stability tests showed that SE decreased from 32 to 28 dB after four months under ambient storage, with no major thermal decomposition below 200 °C (Supplementary Fig. 15). However, humidity-induced weakening of PPy–dopant interactions may cause conductivity drift*[44]*, so long-term humid-environment and cyclic hygrothermal stability remains to be established. Moisture-barrier encapsulation and dopant engineering may address this limitation*[45,46]."

Comments #2-11:

The kirigami rule "Lc < λ/4" is good, but it would help to show either a quick derivation/intuition or cite a key reference for aperture/cut scattering criteria. Also specify which wavelength you used (free space at mid-band or waveguide?).

Our response: Thank you for this comment. We have clarified both the physical basis of the kirigami criterion and the wavelength definition. In this work, $L_c < \lambda_0/4$ is used as a conservative practical design rule to keep each kirigami slit electrically subwavelength and well below the first slot/aperture resonance scale (on the order of $\lambda_0/2$), thereby limiting aperture-induced scattering/transmission. Here, λ_0 refers to the free-space wavelength, not the guide wavelength, although the EMI measurements were performed using the rectangular-waveguide method. This is because the criterion concerns the electrical size of the slit itself rather than the axial phase period of the guided mode; using $\lambda_0$is also the more conservative choice because $\lambda_g > \lambda_0$in the X-band TE_{10} waveguide. To ensure validity across the full X band, we defined the criterion using the upper band edge (12.4 GHz), which gives the shortest wavelength: $\lambda_0 = 24.18$ mm and $\lambda_0/4 = 6.04$ mm. Therefore, both kirigami cut lengths used here (2.4 and 4.8 mm) satisfy this condition throughout 8.2–12.4 GHz. (See reference: doi:10.1103/PhysRev.66.163., *Phys. Rev.* 1944, **66**, 163–182 (1944); doi:10.1063/1.1697868**,** *J. Appl. Phys.1948,* **19**, 24–38)

Our revisions to the manuscript:

We revised the kirigami discussion in Section 5 to state explicitly that the rule is $L_c < \lambda_0/4$, where λ_0 is the free-space wavelength evaluated at 12.4 GHz for the X-band waveguide measurement, and we added a brief physical explanation linking this rule to suppression of slot/aperture scattering. We also added the same clarification in the Methods section on EMI shielding measurements and in the caption of Supplementary Fig. 25, and inserted key references on classical aperture/slot theory.

On Page 12, Line 451-453, we modified the sentences as follows:

"*The slit geometry was chosen conservatively to minimize slit-induced transmission in the X band while permitting stretchability (Methods and Supplementary Fig. 25)*[51,52]."

On Page 25, Line 823-827, we added:

"*For the kirigami samples, the wavelength in the criterion* $L_c < \lambda_0/4$ *refers to the free-space wavelength* λ_0*, not the guide wavelength* λ_g*. We used the upper X-band frequency (12.4 GHz) to define a conservative bound, giving* $\lambda_0/4 = 6.04$ *mm; thus, both kirigami patterns used here (*$L_c = 2.4$ *and 4.8 mm) satisfy this condition throughout 8.2–12.4 GHz*[51,52]."

In the Supplementary Information, we have added the statement to the caption for Supplementary Fig. 25 on Page 26:

"*Periodic straight-line patterns created by laser cutting were designed with cut length* L_c *below one-quarter of the free-space wavelength at the upper band edge (f = 12.4 GHz,* $\lambda_0/4 = 6.04$ *mm) of the X-band measurement. This conservative rule keeps the slits well below the first slot/aperture resonance scale (*$\sim \lambda_0/2$*) and thereby limits aperture-induced scattering/transmission while preserving shielding performance*."

Comments #2-12:

There are several spots where phrasing/notation could be tightened for precision:
o Use consistent band naming (X/Ku/K/Ka) and frequency ranges everywhere.
o Define "low-σ face"/"high-σ face" once, early, and keep consistent.
o Consider changing "low first derivate" → "low first derivative" (typo) and check derivative discussion wording for clarity.

Our response: Thank you so much for this careful comment. In the revised manuscript, we standardized the band labels and frequency ranges throughout the text and figure captions as X (8.2–12.4 GHz), Ku (12.4–18.0 GHz), K (18.0–26.5 GHz), and Ka (26.5–40.0 GHz). We also define the PPy-rich/top surface once, early in the manuscript, as the high-σ face, and the opposite PPy-poor/bottom surface as the low-σ face, and use these terms consistently thereafter. In addition, we corrected the typo "low first derivate" and rewrote the derivative discussion.

Our revision to the manuscript:

We made the following revisions.

1. On Page 24, Line 813-815, we noted the band naming and frequency range:

"…, *standard rectangular waveguides corresponding to the X (8.2-12.4 GHz), Ku (12.4-18.0 GHz), K (18.0-26.5 GHz), and Ka (26.5-40.0 GHz) bands*."

We checked throughout the manuscript /SI and revised the corresponding wording (including captions of Fig. 4), to keep the notation all consistent.

2. On Page 4, Line 140-142, we added the definition of low-σ / high-σ faces:

"*Hereafter, the PPy-rich and PPy-poor surfaces are denoted as the high-σ and low-σ faces, respectively, where σ is the electrical conductivity*."

We checked through the manuscript/SI and kept consistent of this term standardized.

3. We have corrected the typo of "derivate", checked through the manuscript/SI and corrected it. In the Supplementary Information, we have revised the sentence in the caption for Supplementary Fig. 8 on Page 9:

"*In the first 1 mm below the top surface, a short reaction (0.75 h) produces a sharper PPy content drop, whereas a prolonged reaction time (4 h) yields a smoother concentration profile over the same region, corresponding to a smaller derivative magnitude and weaker curvature*."

Reviewer #3 (Remarks to the Author):

Summary: This manuscript presents a highly innovative and well-executed study on monolithic all-polymer aerogels with continuous through-thickness conductivity gradients for ultrabroadband, absorption-dominant electromagnetic interference (EMI) shielding. The work combines elegant materials design, meticulous experimental characterization, and robust theoretical modeling. The demonstrated performance, reflection coefficient ($R < 0.1$) and shielding effectiveness ($SE > 30$) dB across 10.2–40 GHz, is exceptional and represents a significant advance over state-of-the-art materials. The inclusion of mechanical robustness and processability further enhances its practical relevance. The manuscript is well-written, logically structured, and the conclusions are supported by the data. A few minor issues remain that should be addressed to improve clarity and completeness.

Our response: We greatly appreciate your positive comments and support for the publication of our work in *Nature Communications*.

Comments #3-1:

Clarify and quantify the gradient-profile fitting ($\sigma(z)=\sigma0 \cdot \exp(-z/\lambda)$). In Fig. 2h,i and Supplementary Fig. 10, the exponential fits appear reasonable, but the manuscript does not report the fitted parameters and uncertainty. Please add text or table in SI listing σ0 and λ for the key samples (e.g., MCA-1, -2, -4, -4*, -88, -75), together with fit quality (R2 and/or RMSE).

Our response: Thank you for this helpful suggestion. To quantify the conductivity-gradient fitting, we added Supplementary Table 1 listing the fitted σ_0 and λ values, and fit quality for all key specimens, including MCA-1, MCA-2, MCA-4, MCA-6, MCA-4*, MCA-88, and MCA-75. The through-thickness conductivity profiles in Fig. 2h,i and Supplementary Fig. 10 were fitted to $\sigma(z) = \sigma_0 \exp(-z/\lambda)$ using nonlinear regression. The table now reports σ_0, λ, and R^2.

To keep the main text concise, we added a sentence in Section 2 directing readers to Supplementary Table 1. Because the same table also summarizes porosity, thickness, and representative EMI metrics, it serves as a compact design table linking fitted gradient parameters to shielding performance.

Our revision to the manuscript/SI:

On Page 8, Line 302-303, we added:

"*The fitted σ_0 and λ values, together with porosity, thickness, and representative shielding metrics, are summarized in Supplementary Table 1*."

Comments #3-2:

The derivative analysis is conceptually helpful for linking diffusion–reaction to gradient formation, but it reads overly technical for the main narrative. Consider moving the detailed derivative curves and extended mathematical discussion to the SI, while keeping a short, intuitive explanation in the main text emphasizing penetration depth, σ0, and λ.

Our response: Thank you for your suggestion. We agree. We have streamlined the main narrative and kept only the physical interpretation in the main text. The detailed derivative curves and derivative-based discussion have been moved to Supplementary Fig. 8.

Our revision to the manuscript:

On Page 6, Line 210-214, Fig. 2f-g discussion, we modified the following sentence:

"*The simulated PPy concentration profiles (solid lines in Fig. 2f) align with the measured data (Supplementary Fig. 7). Longer diffusion/reaction time increases the PPy penetration depth and broadens the gradient, whereas lower scaffold porosity confines PPy to a shallower depth and produces a steeper profile (Supplementary Fig. 8).*"

In the Supplementary Information, we have added the sentence in the caption for Supplementary Fig. 8 on Page 9:

"*In the first 1 mm below the top surface, a short reaction time (0.75 h) produces a sharper PPy-content drop, whereas a prolonged reaction time (4 h) yields a smoother concentration profile over the same region, corresponding to a smaller derivative magnitude and weaker curvature.*"

Comments #3-3:

The notation MCA-4* is introduced in Fig. 3 and used before its meaning becomes clear in the later section. Please define MCA-4* in the figure caption or the first in-text mention, including what the asterisk denotes and why it is introduced.

Our response: Thank you for this helpful suggestion. We now define MCA-4* at its first in-text mention and in the Fig. 3 caption. The asterisk denotes the atmosphere-modified 4 h sample, introduced to intentionally reduce the surface conductivity relative to MCA-4 while keeping the same nominal diffusion/reaction time.

Our revisions to the manuscript:

On Page 7, Line 247-250, we modified:

"*MCA-4* denotes an intentionally surface-conductivity-reduced variant of MCA-4, prepared under an oxygen-containing polymerization atmosphere;* σ_0 *decreases to ~350 S* m^{-1} *while λ remains ~450 µm (Supplementary Fig. 10a,c, and Supplementary Table 1).*"

On Page 20, Line 699-700, we added:

"*Here, MCA-4* denotes intentionally reduced surface conductivity relative to MCA-4.*"

Comments #3-4:

Supplementary Table S2 is useful, but comparisons are difficult without thickness and density. Please add: (i) thickness for each benchmark entry (if available) in the references, (ii) density or areal density when reported, and (iii) the frequency band definition used for each metric. Also, please correct the reported bandwidth of this work: the bandwidth corresponding to A > 0.9 should be 29.8 GHz (10.2–40.0 GHz) rather than 3.3 GHz.

Our response: Thank you for the important suggestion. We agree and have revised Supplementary Table S2 (after inserting one more table, now it is named as Supplementary Table S3) to improve the rigor and comparability of the benchmarking analysis. We now include sample thickness and density for each benchmark when reported, and the exact frequency window used in each reference. We have also corrected the bandwidth of this work corresponding to A > 0.9 to 29.8 GHz (10.2–40.0 GHz, low-σ-face incidence).

Comments #3-5:

The phrases "continuous conductivity gradient" and "monolithic gradient" are central but not explicitly defined early. Please add a brief definition in the Introduction, clearly distinguishing them from discrete multilayer/stepwise-gradient designs.

Our response: Thank you for this important suggestion. We have added a brief definition in the Introduction to explicitly distinguish our continuous conductivity gradient and monolithic gradient from discrete multilayer or stepwise-gradient designs."

Our revisions to the manuscript:

On Page 3, Line 92-94, we modified:

"*Here, we develop all-polymer aerogels with monolithic, continuous conductivity gradients (MCAs), rather than stepwise architectures with discrete conductivity transitions and interlayer boundaries. MCAs feature….*"

Comments #3-6:

The GSM results convincingly show that increasing N in stepwise approximations improves performance. To make the "continuous gradient" advantage more practically irreplaceable, I would suggest to **consider adding one layered control sample (e.g., a 3-layer stepwise conductivity-gradient control using the same material system**). This can be achieved by stacking thin layers with controlled PPy contents or by stepwise infiltration/polymerization to create discrete interfaces.

Our response: Thank you for this insightful suggestion. Following the reviewer's recommendation, we prepared an additional three-layer stepwise conductivity-gradient control using the same ANF-PVA/PPy material system and a comparable nominal thickness of ~5 mm. The three layers were assembled in a low-to-high conductivity sequence through the thickness to approximate the continuous gradient.

Under low-σ-face incidence, this three-layer control shows effective X-band shielding with $SE_T \sim 34$ dB, $R \sim 0.18$, and $A \sim 0.82$, with negligible transmission. Thus, the discrete stepwise gradient partially recovers impedance matching and absorption-dominant shielding, but its reflection remains about twice that of monolithic continuous-gradient MCA-4* ($R \sim 0.09$, $A \sim 0.91$). This experimental control is consistent with the GSM finite-N prediction: increasing gradient continuity suppresses reflection, whereas small-N discrete gradients retain residual impedance discontinuities.

We added these data to Supplementary Fig. 19 and revised the theoretical-modelling section and Methods accordingly.

Our revision to the manuscript:

On Page 9, Line 359-362, we added:

"*An experimentally implemented three-layer stepwise-gradient control shows intermediate performance (R~0.18, A~0.82, SE_T~34 dB; Supplementary Fig. 19), confirming stepwise gradients only partially recover the impedance-matching benefit of a continuous gradient.*"

On Page 23, Line 758-762, method section, we added:

"*For the three-layer stepwise conductivity-gradient control, three ANF-PVA-PPy layers with different conductivities were prepared from the same material system and assembled in a low-to-high conductivity sequence through the thickness to approximate the continuous conductivity profile. The total thickness of the layered control was kept at ~5 mm for fair comparison in waveguide EMI measurements and simulation.*"

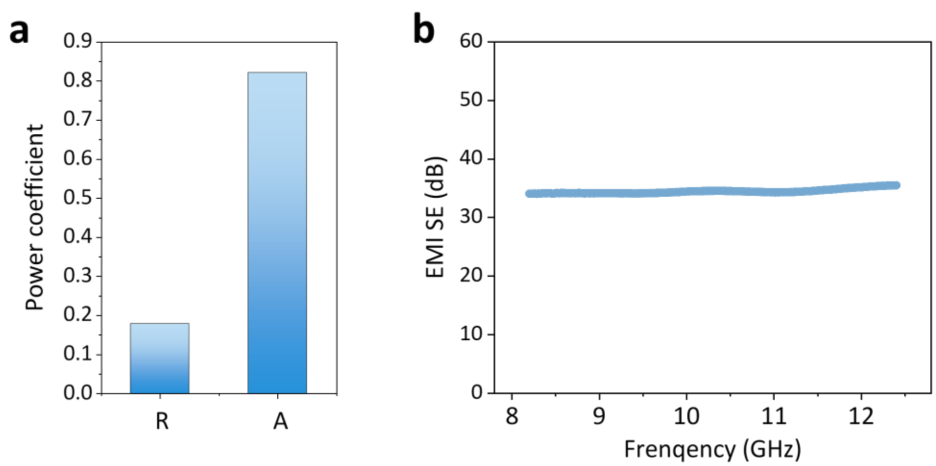

Supplementary Fig. 19 EMI shielding performance of a 3-layer stepwise conductivity-gradient control using the same ANF-PVA/PPy material system. **a.** Power coefficients R and **A** of the 3-layer stepwise conductivity-gradient control under incidence from the low-σ face (transmission is negligible). **b.** EMI shielding effectiveness (SE) of the same sample across the X band (8.2–12.4 GHz). The 3-layer stepwise control approximates the continuous conductivity profile with three discrete conductivity levels and exhibits effective shielding (SE_T ~ 34 dB) together with absorption-dominant behavior (*R* ~ 0.18, *A* ~ 0.82), while still showing higher reflection than the monolithic continuous-gradient MCA-4*.

Comments #3-7:

Unify the naming and definition of λ. The manuscript refers to λ as "decay coefficient/decay character/decay coefficient." Please standardize to same term (e.g., decay length) and specify units (μm or mm), and the z-axis direction at first use (define z=0 at which surface, and which side is the incident face).

Our response: Thank you for this important suggestion. We have standardized λthroughout the manuscript and SI as the characteristic decay length. At the first use, we now define the fitted conductivity profile as $\sigma(z) = \sigma_0 \exp(-z/\lambda)$, where $z = 0$ is located at the high-σ face,z increases from the high-σ face toward the low-σ face, σ_0 is the conductivity at $z = 0$, and λ is the characteristic decay length reported in μm.

We also clarified the incidence convention: unless otherwise stated, EMI measurements are performed under low-σ face incidence, meaning that EMWs enter from the $z = d$side, opposite to $z = 0$. All previous inconsistent terms such as "decay coefficient" or "decay character" have been replaced by "characteristic decay length." To avoid notation ambiguity, electromagnetic wavelengths are denoted as λ_0 or λ_g, whereas λ is reserved for the conductivity decay length.

Our revisions to the manuscript/SI:

On Page 6, Line 232-235, we modified:

"*The through-thickness conductivity profile can be fitted by $\sigma(z) = \sigma_0 \exp(-z/\lambda)$, where σ_0 is the conductivity at the high-σ surface, z is the depth measured from that surface towards the low-σ face ($z = 0$ at the high-σ face), and λ (μm) is the characteristic decay length (Supplementary Fig. 10)*."

On Page 8, Line 284-287, we modified:

"*We next characterized the X-band shielding response across a library of MCAs (thickness ~5 mm) with varied conductivity gradients (MCA-1, -2, -4, -6, -88, -75, and -4*; Fig. 3e-g). The depth-dependent conductivity σ(z) is described by the exponential profile $\sigma(z)=\sigma_0 \exp(-z/\lambda)$ defined above*."

In the Supplementary Information, we have modified the sentence in the caption for Supplementary Fig. 10 on Page 11:

"*Symbols represent experimental data and dashed lines are fits to $\sigma(z)=\sigma_0 \exp(-z/\lambda)$, where σ_0 is the surface conductivity at $z = 0$, λ is the characteristic decay length (μm), and z is measured from the high-σ surface toward the low-σ surface*."

We also revised the inset text in Supplementary Fig. 10a to ensure that the notation for λ is consistent and clear.

Comments #3-8:

Fix symbol formatting consistency and ensure consistent italicization and symbol style throughout, including main texts, methods and supplementary table. Keep the font size and alignment consistent in Supplementary Table 2.

Our response: Thank you for this careful suggestion. We have carried out a full notation and formatting audit across the main text, methods, equations, figure captions, and supplementary tables. Mathematical variables are now italicized consistently, units and standard abbreviations are kept in upright roman, and symbol usage is standardized throughout. Supplementary Table S2 has also been reformatted with uniform font size, alignment, and unit presentation. These formatting revisions improve readability and consistency but do not affect any data, analysis, or conclusion.

Comments #3-9:

In addition to the quantitative parameters (σ0, λ), add a short engineering-style statement summarizing the design rule to improve readability, e.g., lower σ0 improves impedance matching at the incident surface; moderate λ enables gradual transition; excessively small/large λ degrades matching or absorption distribution.

Our response: Thank you for this helpful suggestion. To improve readability, we have added a concise engineering-style design rule that distills the σ_0–λ map into a practical guideline for low-reflection, absorption-dominant shielding.

Our revisions to the manuscript:

On Page 10, Line 375-388, we modified:

"*At fixed thickness (d = 5 mm), 10 GHz, under low-σ-face incidence, the GSM yields a design map in the explored σ_0−λ space for SE_T, A, T, and R (Fig. 4f,g and Supplementary Fig. 20). Within this range, SE_T increases monotonically with σ_0 or λ (Fig. 4f, Supplementary Fig. 20a), as higher conductivity loading and longer conductive penetration suppress transmission*[48]*. However, the A and R responses are non-monotonic. R and A maps show that high-A/low-R window ($A>0.9$ or $R<0.1$) emerges only at intermediate values of σ_0 and λ (Fig. 4g, Supplementary Fig. 20b,d). Too low σ_0 or too small λ weakens the distributed in-depth loss and leaves transmission insufficiently suppressed, whereas too high σ_0 or too large λ may reintroduce the entrance mismatch and reflection. Thus, the optimal design requires simultaneous entrance matching and internal dissipation. The experimentally optimized MCA-4* falls within this window, consistent with its low R and high SE_T. The GSM thus provides a quantitative basis for optimizing experimentally accessible σ_0–λ combinations, in qualitative agreement with the experimental MCA library.*"